

Phonon-induced Floquet second-order topological phases protected by space-time symmetries

Swati Chaudhary,^{1,*} Arbel Haim,^{1,2,†} Yang Peng,^{1,2,3,‡} and Gil Refael¹

¹*Institute of Quantum Information and Matter and Department of Physics,
California Institute of Technology, Pasadena, CA 91125, USA*

²*Walter Burke Institute for Theoretical Physics, California Institute of Technology, Pasadena, CA 91125, USA*

³*Department of Physics and Astronomy, California State University, Northridge, California 91330, USA*

The co-existence of spatial and non-spatial symmetries together with appropriate commutation/anticommutation relations between them can give rise to static higher-order topological phases, which host gapless boundary modes of co-dimension higher than one. Alternatively, space-time symmetries in a Floquet system can also lead to anomalous Floquet boundary modes of higher co-dimensions, presumably with alterations in the commutation/anticommutation relations with respect to non-spatial symmetries. We show how a coherently excited phonon mode can be used to promote a spatial symmetry with which the static system is always trivial, to a space-time symmetry which supports non-trivial Floquet higher-order topological phase. We present two examples – one in class D and another in class AIII where a coherently excited phonon mode promotes the reflection symmetry to a time-glide symmetry such that the commutation/anticommutation relations between spatial and non-spatial symmetries are modified. These altered relations allow the previously trivial system to host gapless modes of co-dimension two at reflection-symmetric boundaries.

Introduction.— The topology of electronic band structures of crystals is largely restricted by the existing symmetries [1–8], and its nontriviality is reflected in the presence of gapless modes located at the crystal boundaries [9–13]. For example, in topological insulators [14–16], where the band topology respects only nonspatial symmetries, such as the time-reversal, particle-hole, and chiral symmetries, the boundary modes are of codimension one (the codimension is the difference between the bulk dimension and the dimension along which the gapless modes propagate).

Recently, systems [17–23] were theoretically proposed to support gapless modes of higher codimensions, because of the additional spatial symmetries coexisting with the nonspatial ones. The order of such higher-order topological insulators is given by the codimension of the boundary modes. On the experimental side, codimension-two boundary modes are observed mostly in metamaterials, such as electric circuits [24], photonic [25] and phononic [26–28] systems. The electronic second-order topological insulator is only realized in Bismuth [29].

If a spatial symmetry coexists with nonspatial symmetries, the symmetry operator of the former can either commute or anticommute with the ones of the latter [7, 8]. Therefore, the coexistence of a certain spatial symmetry alone is not enough to guarantee the possibility of having a nontrivial band topology, but with appropriate commutation or anticommutation relations between the spatial and nonspatial symmetry operators.

Very recently, it was demonstrated that in a periodically driven system, a new space-time symmetry, such as time-glide or time-screw can emerge, if the system is invariant under reflection or two-fold rotation, together with a half-period time translation [30]. As far as topological classification is concerned, such a space-time

symmetry can lead to a nontrivial Floquet band topology, in the same way as its spatial counterpart does in a static system, except for a possible alternation of the commutation/anticommutation relations with respect to the nonspatial symmetries [31, 32].

This result leads to the following interesting question. When the commutation/anticommutation relation alternation does occur, is it able to periodically drive an initially topological trivial system, whose spatial symmetry does not have appropriate relations with respect to the nonspatial symmetries, into a nontrivial Floquet higher-order topological insulator?

In this work, we answer this question by considering phonon-assisted space-time engineering, which promotes the spatial symmetry (such as reflection) of a static system into a space-time symmetry (such as time-glide), without changing the symmetry operator. In this way, the relations with respect to the nonspatial symmetries that are inappropriate for the spatial symmetry, would become otherwise appropriate for the space-time symmetry.

Phonon-assisted space-time engineering.— One assumption in the electronic band structure of a crystal is that the lattice is rigid, with ions fixed to their equilibrium positions. The success of this assumption in characterizing lots of properties of materials is that the energy due to lattice vibrations or phonons is much smaller compared to the electronic energy at the equilibrium lattice configuration.

However, it is known that a coherently excited and macroscopically occupied phonon mode can result in ions moving collectively [33]. When the material is in such a state, the electrons will experience a periodically oscillating ionic potential which can no longer be neglected. Indeed, such a phonon driven Floquet topological

insulator based on graphene has been proposed recently in Ref. [34].

It is known that the symmetries of a crystal in equilibrium with a rigid lattice configuration are described by the space group of the lattice. The normal modes of the lattice vibrations, namely, the phonons, form the irreducible representations of this group. To be more specific, consider an order-two point group operation \hat{g} which squares to identity; the phonon modes must have a definite parity under this operation. Whereas the oscillating potential generated by the even-parity phonon is invariant under such a point group operation at arbitrary times, the one generated by an odd-parity phonon breaks this point group symmetry. Nevertheless, the time-dependent potential $V(\mathbf{r}, t)$ generated by the latter acquires the space-time symmetry, given by $V(\hat{g}\mathbf{r}, t) = V(\mathbf{r}, t + T/2)$, where \mathbf{r} and t are the spatial and temporal coordinates, and T is the oscillation period for the phonon. Hence, we have managed to promote a spatial order-two symmetry described by \hat{g} , to a space-time symmetry described by the same operator, by coherently exciting a phonon mode that is odd under \hat{g} . This is an example of phonon-assisted space-time engineering.

In this manuscript, we provide two examples in which by promoting a spatial symmetry with operator \hat{g} to a space-time symmetry, the commutation relations between \hat{g} and nonspatial symmetries become appropriate for supporting a nontrivial (Floquet) topological phase, whereas only a trivial phase exists in a \hat{g} -symmetric static system. In the supplemental material [35], we list all possibilities of realizing a topological nontrivial Floquet phase from a static trivial system by such phonon-assisted space-time engineering.

2D system in class D/BDI– It is known that in the presence of reflection symmetry, class D or BDI exhibit topological behavior characterized by a mirror topological invariant whenever the reflection operator (described by M) commutes with the particle-hole operator (C) (Table II in the Supplemental material). We demonstrate that a phonon drive can be used to turn a trivial static system with $\{C, M\} = 0$ into non-trivial Floquet topological phase.

Consider a tight-binding model with nearest-neighbor hopping, t_0 , on a two-dimensional square lattice placed in the proximity to a s-wave superconductor described by the Bloch hamiltonian

$$H_0(\mathbf{k}) = (m_0 - 2t_0 \cos k_x - 2t_0 \cos k_y)\tau_z + \Delta\tau_x + b\sigma_x, \quad (1)$$

where σ and τ are Pauli matrices acting on spin and particle-hole degree of freedom respectively. Particle-hole symmetry is given by $C = \tau_y\sigma_y$ and reflection is given by $M = \sigma_x$ flipping the coordinates in the y direction. This also has a time-reversal symmetry given by $T = \mathbb{I}$ but it is not relevant for our purpose as the commutation relation with the time-reversal operator cannot be altered. Let

us consider the effect of a reflection-symmetry breaking phonon which produces a time-dependent Rashba SOC given by :

$$H(\mathbf{k}, t) = 2\alpha_0 \cos \omega t (\sin k_x \sigma_y - \sin k_y \sigma_x) \tau_z. \quad (2)$$

An example for a phonon mode generating such a term is described in the next section.

The full hamiltonian $H_0(\mathbf{k}) + H(\mathbf{k}, t)$ has a time-glide symmetry with reflection $M = \sigma_x$, promoted from the static reflection symmetry. The role of this periodic drive on topological behavior can be understood better by considering the frequency-domain formulation of the Floquet problem and restrict to the two Floquet-zone sector [31, 32]. This two-by-two enlarged Hamiltonian reads

$$\mathcal{H}(\mathbf{k}) = \begin{pmatrix} H_0(\mathbf{k}) + \frac{\omega}{2} & H_1 \\ H_1 & H_0(\mathbf{k}) - \frac{\omega}{2} \end{pmatrix} \quad (3)$$

where $H_n = \frac{1}{T} \int_0^T H(t) e^{-in\omega t} dt$.

This hamiltonian has particle-hole symmetry given by $\mathcal{C} = \sigma_y \tau_y \rho_x$ and reflection $\mathcal{R} = \sigma_x \rho_z$ where we have introduced a set of Pauli matrices $\rho_{x,y,z}$ for the new spinor degree of freedom in the extended Floquet basis. It belongs to class D and has appropriate commutation relations. Its topological behavior can thus be understood in terms of mirror topological invariant \mathbb{Z}_2 (see Supplemental Material). The resulting band structure is shown in Fig. 1 with periodic boundary conditions in one direction. It features gapless modes around quasienergy $\omega/2$ for periodic BC in y direction whenever \mathbb{Z}_2 is non-trivial. Now, if we modify the boundary such that it gives rise to an effective reflection symmetric-breaking mass term, the edge modes are replaced by the hinge modes on reflection-symmetric corners as shown in Fig. 2.

A toy model for phonon induced Rashba SOC– The main ingredients needed for a Rashba SOC are the on-site π - σ spin dependent interactions and the nearest-neighbor π - σ hopping between same parity orbitals. The spin-dependent on-site π - σ interaction occurs naturally because of an $\mathbf{L} \cdot \mathbf{S}$ term, and the nearest neighbor hopping between π - σ orbitals of same parity can be facilitated by the opposite parity orbitals or by ligands. For example, in graphene the intrinsic Rashba SOC occurs because of nearest-neighbor hopping between p and s/d orbitals [36, 37]. Furthermore, the ligands can mediate a nearest-neighbor π - σ hopping which depends on their position, and thus can give rise to a time-dependent Rashba SOC when they oscillate. Consider that each site of our square lattice model considered above has three non-degenerate p orbitals where neighboring p_z orbitals hybridize to form π bands and rest of the orbitals form σ bands. These π and σ orbitals interact via $\mathbf{L} \cdot \mathbf{S}$ coupling (Table I). Furthermore, assume that an additional atom (which we call ligand) with active s orbitals is located between two lattice sites as shown in Fig. 3. This

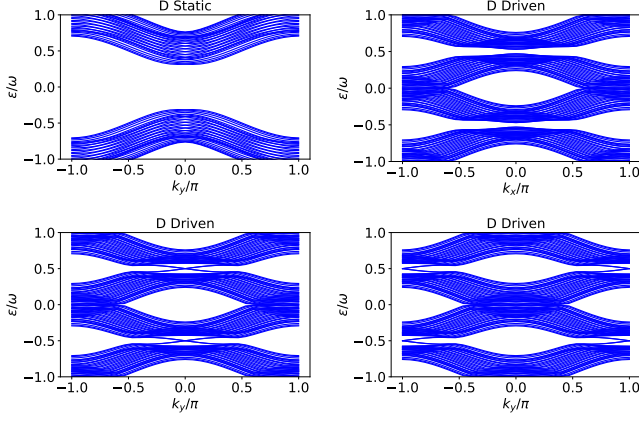


FIGURE 1. Band structure for $m_0 = \omega/2 + 1$, $\Delta = 0.9$, $\omega = 4.8$, $L = 15$, $b = 0.15$, and $\alpha_0 = 0.5$ with periodic boundary conditions in one direction. In the last plot $m_0 = -\omega/2 - 1$ and this change of sign results in a shift in the position of gapless mode from $k_y = 0$ to $k_y = \pi$ ($\Delta = 0.5$, $\alpha_0 = 1.0$ is shown in Supplemental material). (All energies are in units of t_0 .)

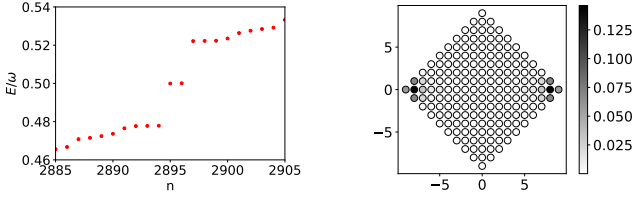


FIGURE 2. Left Panel : Energy spectrum of the Floquet hamiltonian with H_1 of Eq. 2 around quasienergy $\omega/2$ for open boundary conditions in both directions with reflection-symmetry broken edges. Right panel : Support of the hinge mode for these boundary conditions corresponding to quasienergy $\omega/2$.

arrangement essentially forms a Lieb lattice. When the ligand is displaced in z direction, it induces a hopping between π and σ orbitals. When combined with on-site interaction $\mathbf{L} \cdot \mathbf{S}$ between π and σ orbitals, it produces an effective spin-dependent hopping between π orbitals

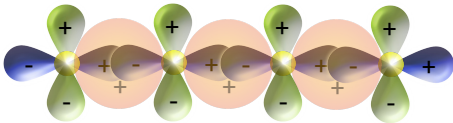


FIGURE 3. This figure shows the p_x (green) and p_z (blue) orbitals of the two dimensional square lattice along the x direction with s orbitals of the ligands shown in orange color. When the ligand ion is displaced in z direction, it induces a hopping between p_x and p_z orbitals.

given by :

$$\begin{aligned} \langle p_{z,i,j} | H_{\text{eff}} | p_{z,i+1,j} \rangle &= t_{zz} + \frac{1}{\epsilon_{zx}} t_{i,i+1}^{z,x} \langle p_{x,i+1} | \mathbf{L} \cdot \mathbf{S} | p_{z,i+1} \rangle \\ &= t_{zz} + i \frac{t_u \zeta}{\epsilon_{zx}} \sigma_y, \end{aligned} \quad (4)$$

where $t_{zz} = t_0$ is the direct hopping between two p_z orbitals, ϵ_{zx} is the energy gap between p_z and p_x orbitals, and t_u is the hopping between $p_{z,i}$ and $p_{x,i+1}$ orbital induced by s orbitals of the ligand. Similarly, we

Orbital	p_x	p_y	p_z
p_x	0	$-i\zeta s_z$	$i\zeta s_y$
p_y	$i\zeta s_z$	0	$-i\zeta s_x$
p_z	$-i\zeta s_y$	$i\zeta s_x$	0

TABLE I. Matrix element of $\mathbf{L} \cdot \mathbf{S}$ operator for p orbitals.

can get a σ_x dependent hopping in the y direction. For a small lattice displacement, this ligand-induced hopping $t_u \approx \left(\frac{u(t)}{L} t_{sp\sigma} \right) t_{sp\sigma} / \epsilon_{sp}$ where $t_{sp\sigma}$ is the hopping between $p_{x/y}$ orbital and the s orbital of the ligand, ϵ_{sp} is the energy separation between s and p orbitals, L is the distance of the ligand from the neighboring lattice site, and $t_{sp\sigma} u(t)/L$ is the hopping between the π orbital and s orbital of the ligand which comes into picture only when the lattice displacement $u(t)$ is non-zero [38]. It gives rise to a time-dependent Rashba SOC which can be controlled by the lattice vibrations associated with the ligand motion. For a coherent phonon, $u(t) \approx u_0 \cos \omega t$ where the ratio u_0/L can be as large as 0.1 in certain cases [39, 40]. The ligand-induced hopping t_u depends on a lot of factors like the phonon amplitude, energy separation ϵ_{sp} , and the hopping $t_{sp\sigma}$ which can be much larger than the π hopping t_{zz} . Depending on the ligand species, $\epsilon_{sp} \approx 1-10\text{eV}$, and thus the effective hopping $t_{sp\sigma}^2 / \epsilon_{sp}$ can be anywhere between $0.1t_{zz}$ and $5t_{zz}$ since the ratio $t_{sp\sigma}/t_{zz} \approx 1-10$ usually. This rough estimate indicates that the ligand-induced hopping t_u can be anywhere between $0.1t_{zz}$ and t_{zz} , and thus the drive strength $\alpha_0 \approx (0.1 - 1)t_{zz}\zeta/\epsilon_{zx}$ can be of the same order as t_{zz} if the spin-orbit coupling ζ is comparable to the energy separation between π and σ orbitals.

2D system in class AIII. – It is known that insulators in class AIII respecting the chiral symmetry (described by S) alone have only the trivial band topology. When a unitary reflection symmetry (described by M , with $M^2 = 1$) exists, a \mathbb{Z} topological classification is possible only when $[S, M] = 0$ [7, 8].

Consider a tight-binding model for Bernal-stacked bilayer graphene-like lattice with nearest-neighbor intra-layer hopping for all sites and nearest-neighbor inter-layer hopping between non-dimer sites as shown in Fig. 4. For periodic boundary conditions, the corresponding Bloch

hamiltonian reads

$$\begin{aligned}
 H_0(\mathbf{k}) = & t_a \tau_x + 2t_b \left(\cos \frac{k_x}{2} \cos \frac{\sqrt{3}k_y}{2} \tau_x + \cos \frac{k_x}{2} \sin \frac{\sqrt{3}k_y}{2} \tau_y \right) \\
 & + \left(t_w \cos \frac{k_x}{2} \cos \frac{\sqrt{3}k_y}{2} + \frac{t_{w2}}{2} \cos \sqrt{3}k_y \right) (\sigma_x \tau_x - \sigma_y \tau_y) \\
 & + \left(t_w \cos \frac{k_x}{2} \sin \frac{\sqrt{3}k_y}{2} + \frac{t_{w2}}{2} \sin \sqrt{3}k_y \right) (\tau_x \sigma_y + \tau_y \sigma_x) \\
 & + t_3 (\tau_x \sigma_x + \sigma_y \tau_y)
 \end{aligned} \tag{5}$$

where τ and σ now operate on sublattice and layer degrees of freedom, respectively. It has chiral symmetry $S = \tau_z$ and mirror-symmetry $M = \sigma_x \tau_x$ flipping the coordinates in the y direction.

When a phonon mode is coherently excited such that the atoms A_1 and B_2 oscillate out of phase along the x direction, the hopping for the nearest neighbors in \mathbf{a}_1 and \mathbf{a}_2 direction as shown in Fig. 4 acquires an additional contribution

$$\begin{aligned}
 H(t) = & \beta(t) \sum_{\mathbf{r}_i, \alpha=1,2} (a_{\alpha, \mathbf{r}_i}^\dagger b_{\alpha, \mathbf{r}_i + \mathbf{a}_1} - a_{\alpha, \mathbf{r}_i}^\dagger b_{\alpha, \mathbf{r}_i + \mathbf{a}_2} + h.c) \\
 & + \gamma(t) \sum_{\mathbf{r}_i} (a_{1, \mathbf{r}_i}^\dagger b_{2, \mathbf{r}_i + \mathbf{a}_1} - a_{1, \mathbf{r}_i}^\dagger b_{2, \mathbf{r}_i + \mathbf{a}_2} + h.c),
 \end{aligned} \tag{6}$$

and thus adds

$$\begin{aligned}
 H(\mathbf{k}, t) = & \beta(t) \left(-\sin \frac{k_x}{2} \cos \frac{\sqrt{3}k_y}{2} \tau_y + \sin \frac{k_x}{2} \sin \frac{\sqrt{3}k_y}{2} \tau_x \right) \\
 & + \gamma(t) \sin \frac{k_x}{2} \cos \frac{\sqrt{3}k_y}{2} (\sigma_x \tau_y + \sigma_y \tau_x) \\
 & + \gamma(t) \sin \frac{k_x}{2} \sin \frac{\sqrt{3}k_y}{2} (\sigma_x \tau_x - \sigma_y \tau_y)
 \end{aligned} \tag{7}$$

to Bloch hamiltonian $H_0(\mathbf{k})$ where a/b refers to A and B sublattice sites, α indicates the layer index, and $\beta(t)$ and $\gamma(t)$ are proportional to the lattice displacement $u(t)$ for small phonon amplitudes. Their magnitude can be estimated as $\beta(t) \approx \eta u(t) t_0 / d_0$, where $\eta \approx 1-4$, t_0 is the static hopping between two sites, and d_0 is the equilibrium separation between two sites, as the hopping in a tight binding model usually changes by a factor of $\left(\frac{d_0}{d_0+u}\right)^\eta$ [41]. For a coherent phonon, the lattice displacement $u(t) \approx u_0 \cos \omega t$ which gives $\beta(t) = \beta_0 \cos \omega t$, and thus $H(\mathbf{k}, t) = H_1(\mathbf{k}) \cos \omega t$. For a lattice displacement of 5-10%, the drive strength β_0 and γ_0 can be anywhere between 5-40% of the static hopping amplitude t_0 .

Now, the two-by-two enlarged hamiltonian (Eq.3) has a chiral symmetry, $\mathcal{S} = S \rho_x$ and a reflection symmetry realized by $\mathcal{R} = M \rho_z$. Since $[\mathcal{S}, \mathcal{R}] = 0$, we can

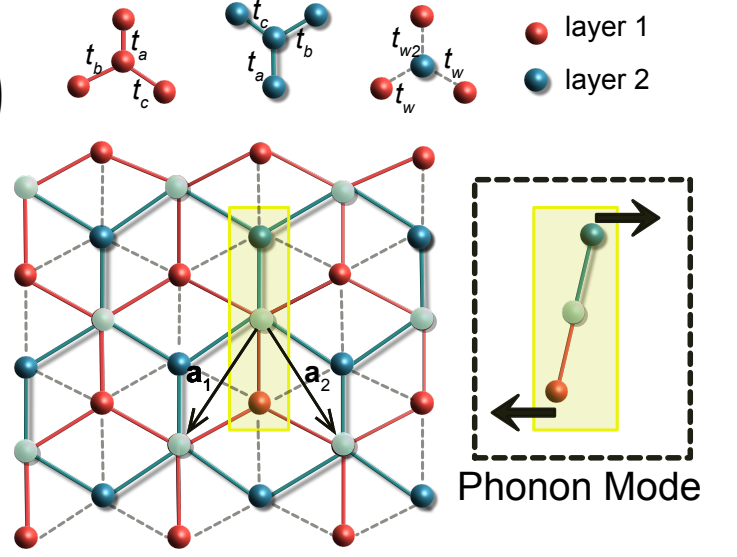


FIGURE 4. A schematic for A-B stacked bilayer honeycomb lattice with nearest-neighbor intra-layer (solid lines) and inter-layer (dashed lines) hopping. The unit cell of the triangular lattice is shown in a yellow box. The dimer sites (shown in light blue color) don't participate in inter-layer hopping. The right inset shows the phonon mode which affects the hopping parameters t_b , t_c , and t_w .

have a nontrivial classification with a mirror \mathbb{Z} topological invariant. In non-trivial regime, it hosts gapless edge modes along y boundaries for the driven system which are protected by reflection-symmetry. These gapless edge modes at $k_y = 0$ co-exist with some gapless bulk modes at arbitrary $\pm k_y$ which are not protected by the reflection-symmetry. These points arise due to bulk-band gap closings which can be removed, for example, by a drive-induced interlayer imaginary hopping between dimers

$$H_I(t) = \lambda(t) \sum (i a_{1, \mathbf{r}_i}^\dagger b_{2, \mathbf{r}_i + \mathbf{a}_1} + i a_{1, \mathbf{r}_i}^\dagger b_{2, \mathbf{r}_i + \mathbf{a}_2} + h.c) \tag{8}$$

which in k space becomes

$$H_I(\mathbf{k}) = \lambda(t) \cos \frac{k_x}{2} \sin \frac{\sqrt{3}k_y}{2} (\sigma_x \tau_x + \sigma_y \tau_y). \tag{9}$$

This kind of hopping might not be so easy to realize but it verifies the fact that these gapless bulk modes are not protected by reflection-symmetry alone. In this case, if we modify the boundary such that it gives rise to an effective reflection symmetric-breaking mass term, the gapless edge modes are replaced by the hinge modes on reflection-symmetric corners as shown in Fig.6. Alternatively, the gapless bulk modes can be gapped by translational-symmetry-breaking perturbation, such as a charge density wave. We discuss this possibility in the Supplemental material.

Conclusions.— We discussed how a phonon drive can be used to promote a static symmetry to a space-time

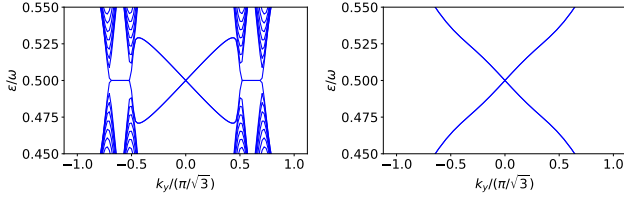


FIGURE 5. Band structure around $\omega/2$ for Floquet hamiltonian (upto two Floquet sectors) without/with imaginary hopping (left/right) of Eq.8. At $k_y = 0$, time-glide symmetry gives rise to two gapless edge modes which co-exist with other gapless modes in the absence of imaginary hopping term. The parameters for left figure are : $t_a = 2.4, t_b = 1.2, t_3 = 0.5, \beta_0 = 0.1, t_w = 0.5, \gamma_0 = 0.5, \omega = 4.4, t_{w2} = 0.1$ and for the right figure $\gamma_0 = 0.8, \lambda = 0.8$.

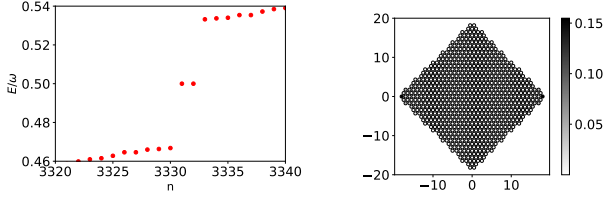


FIGURE 6. Left panel : Energy spectrum of Floquet hamiltonian with H_1 of Eq.8 around quasienergy $\omega/2$ for open boundary conditions with reflection-symmetry breaking term. Right panel : Support of the hinge mode for these boundary conditions corresponding to quasienergy $\omega/2$. The parameters for this figure are : $t_a = 2.4, t_b = 1.2, t_3 = 0.5, t_w = 0.1, \beta_0 = 0.1, \gamma_0 = 0.8, \lambda_0 = 0.8, t_{w2} = 0.1$

symmetry which in turn can allow the system to exhibit a topological classification. Both of these schemes need phonon frequencies to be of the same order as hopping parameter. These phonon frequencies usually depend on the bond strength while the hopping parameter in graphene-like lattices depend on overlap between neighboring π orbitals. This kind of parameter regime can be realized by suppressing the hopping parameter without affecting the bond strengths between neighboring atoms which determine the phonon frequencies. Alternatively, one can consider placing the system on a substrate which binds to different sites such that the phonon frequencies are increased. These lattice models can be possibly realized using covalent organic framework [42, 43] where molecular orbitals play the same role as atomic orbitals in our model and hopping parameters are of the order of 100meV. Similarly, twisted bilayer materials can provide another platform to realize the Class AIII model where hopping parameters can be made comparable to certain phonon frequencies [44, 45].

Acknowledgement.— We acknowledge support from the Institute of Quantum Information and Matter, an NSF Frontier center funded by the Gordon and Betty Moore Foundation, the Packard Foundation, and the Simons foundation. A. H. and Y.P. are grateful to support

from the Walter Burke Institute for Theoretical Physics at Caltech. G. R. is grateful to the support from the ARO MURI W911NF-16-1-0361 Quantum Materials by Design with Electromagnetic Excitation sponsored by the U.S. Army.

* swatich@caltech.edu

† arbelh@caltech.edu

‡ yangpeng@caltech.edu

- [1] A. P. Schnyder, S. Ryu, A. Furusaki, and A. W. W. Ludwig, *Phys. Rev. B* **78**, 195125 (2008).
- [2] A. Kitaev, AIP Conf. Proc. **1134**, 22 (2009).
- [3] S. Ryu, A. P. Schnyder, A. Furusaki, and A. W. Ludwig, *New Journal of Physics* **12**, 065010 (2010).
- [4] A. M. Turner, Y. Zhang, and A. Vishwanath, *Phys. Rev. B* **82**, 241102 (2010).
- [5] T. L. Hughes, E. Prodan, and B. A. Bernevig, *Phys. Rev. B* **83**, 245132 (2011).
- [6] L. Fu, *Phys. Rev. Lett.* **106**, 106802 (2011).
- [7] C.-K. Chiu, H. Yao, and S. Ryu, *Phys. Rev. B* **88**, 075142 (2013).
- [8] K. Shiozaki and M. Sato, *Phys. Rev. B* **90**, 165114 (2014).
- [9] J. C. Y. Teo and C. L. Kane, *Phys. Rev. B* **82**, 115120 (2010).
- [10] C.-K. Chiu, J. C. Y. Teo, A. P. Schnyder, and S. Ryu, *Rev. Mod. Phys.* **88**, 035005 (2016).
- [11] E. Khalaf, *Phys. Rev. B* **97**, 205136 (2018).
- [12] E. Khalaf, H. C. Po, A. Vishwanath, and H. Watanabe, *Phys. Rev. X* **8**, 031070 (2018).
- [13] L. Trifunovic and P. W. Brouwer, *Phys. Rev. X* **9**, 011012 (2019).
- [14] M. Z. Hasan and C. L. Kane, *Rev. Mod. Phys.* **82**, 3045 (2010).
- [15] X.-L. Qi and S.-C. Zhang, *Rev. Mod. Phys.* **83**, 1057 (2011).
- [16] B. A. Bernevig and T. L. Hughes, *Topological insulators and topological superconductors* (Princeton University Press, 2013).
- [17] W. A. Benalcazar, B. A. Bernevig, and T. L. Hughes, *Phys. Rev. B* **96**, 245115 (2017).
- [18] Y. Peng, Y. Bao, and F. von Oppen, *Phys. Rev. B* **95**, 235143 (2017).
- [19] J. Langbehn, Y. Peng, L. Trifunovic, F. von Oppen, and P. W. Brouwer, *Phys. Rev. Lett.* **119**, 246401 (2017).
- [20] W. A. Benalcazar, B. A. Bernevig, and T. L. Hughes, *Science* **357**, 61 (2017).
- [21] Z. Song, Z. Fang, and C. Fang, *Phys. Rev. Lett.* **119**, 246402 (2017).
- [22] F. Schindler, A. M. Cook, M. G. Vergniory, Z. Wang, S. S. Parkin, B. A. Bernevig, and T. Neupert, *Sci. Adv.* **4**, eaat0346 (2018).
- [23] M. Geier, L. Trifunovic, M. Hoskam, and P. W. Brouwer, *Phys. Rev. B* **97**, 205135 (2018).
- [24] S. Imhof, C. Berger, F. Bayer, J. Brehm, L. W. Molenkamp, T. Kiessling, F. Schindler, C. H. Lee, M. Greiter, T. Neupert, *et al.*, *Nature Physics* **14**, 925 (2018).
- [25] C. W. Peterson, W. A. Benalcazar, T. L. Hughes, and G. Bahl, *Nature* **555**, 346 (2018).
- [26] M. Serra-Garcia, V. Peri, R. Süssstrunk, O. R. Bilal, T. Larsen, L. G. Villanueva, and S. D. Huber, *Nature*

and other symmetry operator are also modified, for example the new (effective) operators for time-reversal, charge-conjugation, and chiral symmetry are now given by :

$$\mathcal{T} = \begin{pmatrix} \tau & & & \\ & \tau & & \\ & & \tau & \\ & & & \tau \end{pmatrix}, \mathcal{C} = \begin{pmatrix} & & c \\ & c & \\ c & & \end{pmatrix}, \mathcal{S} = \begin{pmatrix} & & s \\ & s & \\ s & & \end{pmatrix}. \quad (14)$$

Now, the commutation relation between effective different symmetry operators is different from the commutation relation for the static case. This indicates that the effective hamiltonian although belongs to the same AZ class as the static hamiltonian but can allow the existence of a non trivial topological phase (For e.g $\{M, S\} = 0 \implies [\mathcal{R}, \mathcal{S}] = 0$) in the presence of this time-glide symmetry. We are going to exploit this feature in realizing non-topological phase by altering the modified commutation relations which results in a change in topological classification as shown in Table. II. Although, in this work we use a periodic drive to promote reflection symmetry to a time-glide symmetry in two dimensions, the same ideas can be applied to two-fold rotations and inversion symmetry in two and three dimensions and the consequences of such promotions are discussed in table II and table III.

Class	2D		3D	
	Symmetry Promotion	Classification	Symmetry Promotion	Classification
AIII	R_-	\mathbb{Z}	R_+	\mathbb{Z}^2
BDI	R_{+-}	\mathbb{Z}	R_{--}	\mathbb{Z}
D	R_-	\mathbb{Z}_2	R_-	\mathbb{Z}
DIII	R_{+-}	\mathbb{Z}_2	R_{--}	\mathbb{Z}^2
CII	R_{+-}	$2\mathbb{Z}$	R_{++}	\mathbb{Z}_2^2
CI	R_{-+}	$2\mathbb{Z}$	R_{++}	\mathbb{Z}
AIII	C_{2+}	\mathbb{Z}	C_{2-}	\mathbb{Z}^2
BDI	C_{2++}	\mathbb{Z}	C_{2+-}	\mathbb{Z}
DIII	C_{2++}	\mathbb{Z}	C_{2+-}	\mathbb{Z}
CII	C_{2++}	$2\mathbb{Z}$	C_{2+-}	\mathbb{Z}
CI	C_{2++}	$2\mathbb{Z}$	C_{2+-}, C_{2-+}	$\mathbb{Z}, (2\mathbb{Z})^2$

TABLE II. Symmetry promotion from reflection R and two-fold rotation C .

Class	3D	
	Symmetry Promotion	Classification
AIII	I_+	\mathbb{Z}^2
BDI	I_{++}	\mathbb{Z}
D	I_+	\mathbb{Z}
DIII	I_{++}	\mathbb{Z}^2
CII	I_{--}	\mathbb{Z}_2^2
CI	I_{--}, I_{++}	$\mathbb{Z}, (2\mathbb{Z})^2$

TABLE III. Symmetry promotion from inversion I

When the drive is monochromatic, $H_n = 0$ for $|n| > 1$, and thus the above symmetries can be best described in terms of constraints on H_0 and H_1 . In this case, the chiral symmetric hamiltonians satisfy :

$$SH_0(\mathbf{k}, \mathbf{r})S^{-1} = -H_0(\mathbf{k}, \mathbf{r}), \quad SH_1(\mathbf{k}, \mathbf{r})S^{-1} = -H_1^+(\mathbf{k}, \mathbf{r}). \quad (15)$$

Similarly particle-hole symmetry is given by :

$$CH_0^*(\mathbf{k}, \mathbf{r})C^{-1} = -H_0(-\mathbf{k}, \mathbf{r}), \quad CH_1^*(\mathbf{k}, \mathbf{r})C^{-1} = -H_1^+(-\mathbf{k}, \mathbf{r}) \quad (16)$$

and time-glide by :

$$MH_0(k_x, k_y)M^{-1} = H_0(-k_x, k_y), \quad MH_1(k_x, k_y)M^{-1} = -H_1(-k_x, k_y). \quad (17)$$

MIRROR TOPOLOGICAL INVARIANT $M\mathbb{Z}_2$ FOR CLASS D, R_+ IN TWO DIMENSIONS

For class D, when the particle-hole and reflection symmetry operator commute, the different topological phases can be distinguished on the basis of mirror topological invariant $M\mathbb{Z}_2$. This invariant can be calculated at reflection symmetric hyperplanes by first block diagonalizing the hamiltonian in \mathcal{R} basis, and then calculating the \mathbb{Z}_2 invariant for one block. When the reflection operator commutes with the effective particle-hole operator \mathcal{C} , these two blocks do not mix and hence a classification can be made on the basis of this topological invariant for one block. In the main text we considered the undriven model :

$$H_0(k_x, k_y) = m_1\tau_z + \Delta\tau_x + b\sigma_x \quad (18)$$

where $m_1 = m - 2t_0 \cos k_x - 2t_0 \cos k_y$ with a drive of the form :

$$H(t) = 2\alpha_0 \cos \omega t (\sin k_x \sigma_y - \sin k_y \sigma_x) \tau_z = H_1 e^{i\omega t} + H_1^\dagger e^{-i\omega t}. \quad (19)$$

This hamiltonian has a particle-hole symmetry given by $C = \tau_y \sigma_y$ and time-glide with reflection $M = \sigma_x$ about y axis ($y \rightarrow -y$). We can cast it into a more familiar form if we use the eigenstate basis of $m(\mathbf{k})\tau_z + \Delta\tau_x$ which corresponds to a transformation $\tau_z \rightarrow \cos \theta \tau_z - \sin \theta \tau_x$ where $\cos \theta = \frac{m(\mathbf{k})}{\sqrt{m(\mathbf{k})^2 + \Delta^2}}$. In this basis :

$$H_0 = \sqrt{m(\mathbf{k})^2 + \Delta^2} \tau_z + b\sigma_x, \quad (20)$$

and

$$H_1 = 2\alpha_0 (\sin k_x \sigma_y - \sin k_y \sigma_x) \left(\frac{m(\mathbf{k})}{E_k} \tau_z - \frac{\Delta}{E_k} \tau_x \right) \quad (21)$$

where $E_k = \sqrt{m(\mathbf{k})^2 + \Delta^2}$. In this basis, the particle-hole operator $C = \tau_y \sigma_y$ and time-glide $M = \sigma_x$ remains the same. Now the Floquet hamiltonian for photon sectors n and $n+1$ can be written as :

$$H_F(\mathbf{k}) = \begin{pmatrix} E_k \tau_z + \frac{\omega}{2} \mathbb{I} + b\sigma_x & \alpha_0 (\sin k_x \sigma_y - \sin k_y \sigma_x) \left(\frac{m(\mathbf{k})}{E_k} \tau_z - \frac{\Delta}{E_k} \tau_x \right) \\ \alpha_0 (\sin k_x \sigma_y - \sin k_y \sigma_x) \left(\frac{m(\mathbf{k})}{E_k} \tau_z - \frac{\Delta}{E_k} \tau_x \right) & E_k \tau_z - \frac{\omega}{2} \mathbb{I} + b\sigma_x \end{pmatrix}. \quad (22)$$

The topological behavior of this hamiltonian can also be understood by focusing on its inner 4×4 block given by :

$$\mathcal{H}(\mathbf{k}) = \begin{pmatrix} (-E_k + \frac{\omega}{2}) \mathbb{I} + b\sigma_x & \alpha_0 (\sin k_x \sigma_y - \sin k_y \sigma_x) \frac{\Delta}{E_k} \\ \alpha_0 (\sin k_x \sigma_y - \sin k_y \sigma_x) \frac{\Delta}{E_k} & (E_k - \frac{\omega}{2}) \mathbb{I} + b\sigma_x \end{pmatrix} = (-E_k + \frac{\omega}{2}) \rho_z + b\sigma_x + \alpha_0 (\sin k_x \sigma_y - \sin k_y \sigma_x) \frac{\Delta}{E_k} \rho_x \quad (23)$$

where ρ indicates the photon degree of freedom. In this case, the particle-hole symmetry $\mathcal{C} = \sigma_y p_y$ and it has a reflection symmetry $\mathcal{R} = \sigma_x \rho_z$ which commutes with \mathcal{C} , and hence it can be characterized by a mirror \mathbb{Z}_2 invariant. In order to calculate this topological invariant we go to reflection symmetric hyperplanes ($k_y = 0, \pi$) and express this hamiltonian in the basis of M arranged such that first block has eigenvalue +1. The above hamiltonian of Eq. 23 takes the following form :

$$\mathcal{H}(k_x) = \begin{pmatrix} H_+ & \\ & H_- \end{pmatrix} = \begin{pmatrix} -E_k + \frac{\omega}{2} + b & -i\alpha_0 \sin k_x \frac{\Delta}{E_k} & 0 & 0 \\ i\alpha_0 \sin k_x \frac{\Delta}{E_k} & E_k - \frac{\omega}{2} - b & 0 & 0 \\ 0 & 0 & E_k - \frac{\omega}{2} + b & -i\alpha_0 \sin k_x \frac{\Delta}{E_k} \\ 0 & 0 & i\alpha_0 \sin k_x \frac{\Delta}{E_k} & -E_k + \frac{\omega}{2} - b \end{pmatrix} \quad (24)$$

with

$$R = \begin{pmatrix} 1 & & & \\ & 1 & & \\ & & -1 & \\ & & & -1 \end{pmatrix} \text{ and } P = \begin{pmatrix} & -1 & & \\ -1 & & & \\ & & 1 & \\ & & & 1 \end{pmatrix} \quad (25)$$

in the new basis. Now, each block belongs to class D and in order to calculate the mirror \mathbb{Z}_2 invariant we can pick any block. For example if we pick H_+ , then the invariant can be calculated from Pfaffin of H_+ at $k_x = 0, \pi$. At $k_y = 0$, the \mathbb{Z}_2 topological invariant is given by :

$$\eta_{k_y=0} = \text{Sign}[(E_k - \frac{\omega}{2} + b)_{(k_x=0, k_y=0)}(E_k - \frac{\omega}{2} + b)_{(k_x=\pi, k_y=0)}]. \quad (26)$$

Similarly, at $k_y = \pi$

$$\eta_{k_y=\pi} = \text{Sign}[(E_k - \frac{\omega}{2} + b)_{(k_x=0, k_y=\pi)}(E_k - \frac{\omega}{2} + b)_{(k_x=\pi, k_y=\pi)}], \quad (27)$$

and thus the mirror \mathbb{Z}_2 invariant is now given by :

$$\eta_{M\mathbb{Z}_2} = 1 - |\eta_{k_y=0} - \eta_{k_y=\pi}| = \text{Sign}[\eta_{k_y=0}\eta_{k_y=\pi}], \quad (28)$$

and its dependence on m_0 and Δ is shown in Fig. 7. This indicates that if the system size is quite large, we can get a non-trivial phase for a very small value of superconducting gap Δ but for small system sizes we find the gapless edge modes only for $\Delta \approx 0.5$ as the bulk gap becomes very small for lower values of Δ . Although, the topological invariant

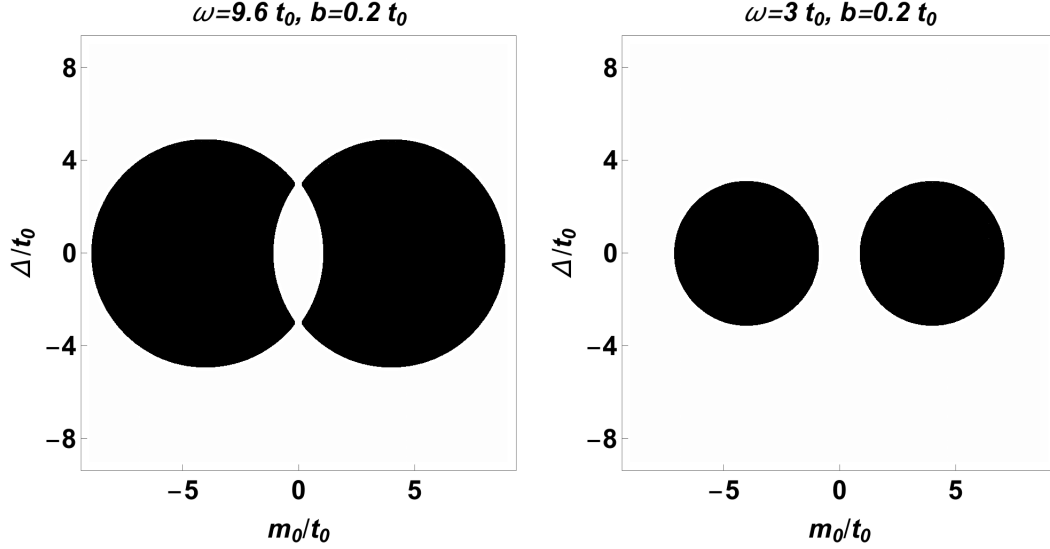


FIGURE 7. Mirror topological invariant $\eta_{M\mathbb{Z}_2}$ on parameters m_0 and Δ for two different values of ω . All parameters are given in units of hopping amplitude t_0 . Black regions indicate the non-trivial region.

is non-trivial for a large range of m and Δ but the system does not seem to exhibit corner modes for small values of Δ . In order to understand the regime for gapless boundary states we study an eightband model which captures the essential features of the above model. This model is given by hamiltonian :

$$H_{\text{eff}} = \begin{pmatrix} H_0 + \frac{\omega}{2} & H_1 \\ H_1^\dagger & H_0 - \frac{\omega}{2} \end{pmatrix} \quad (29)$$

The spectrum of this hamiltonian is shown in Fig. 8 for open boundary conditions. In certain cases, the bulk gap becomes very small and thus the gapless boundary modes or zero energy hinge modes can not be observed for a small system size.

EFFECT OF TRANSLATION-SYMMETRY BREAKING PERTURBATIONS ON GAPLESS BULK MODES AT FLOQUET ZONE BOUNDARIES

We study the effect of a charge-density wave type perturbation in the bilayer graphene model considered above. For each site $\mathbf{R} = n\mathbf{a}_1 + p\mathbf{a}_2$ on the underlying triangular lattice of Fig. 5, we add a term of the form of $A_0 \cos(qp)$ to all the nearest-neighbor hopping in the static and the drive part. We calculate the conductance in y direction for different amplitudes A_0 and wavevector q of this extra term using Kwant [46]. Without this charge-density wave term, the observed conductance has a contribution from both edge and bulk modes at quasienergy $\omega/2$, but this term suppresses the bulk contribution as shown in Fig. 9. In the presence of the charge-density wave perturbation, the conductance is quantized to two which indicates that it arises from the protected edge modes in the presence of a gapped bulk.

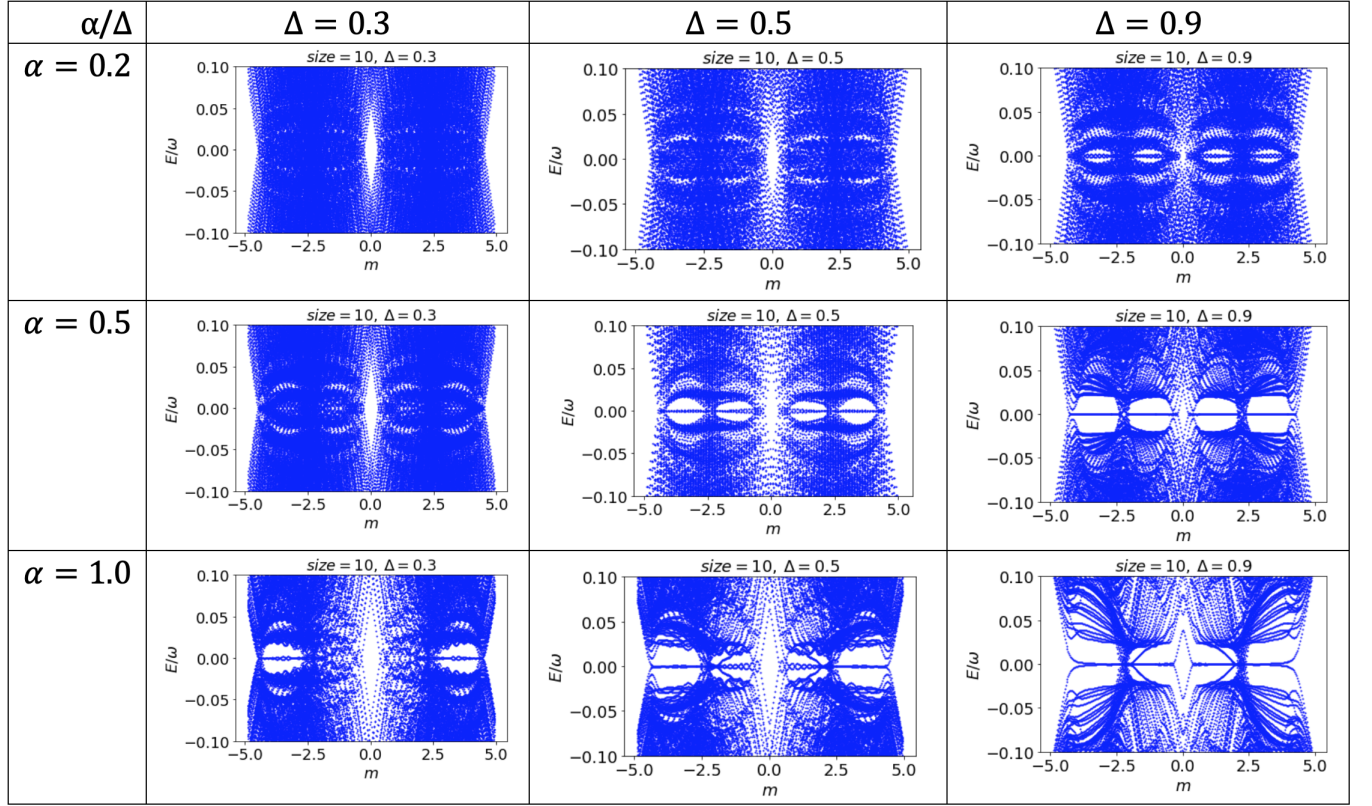


FIGURE 8. Energy spectrum around zero energy as a function of m for an eight band model capturing the main features of the τ_z drive considered in Eq. 29.

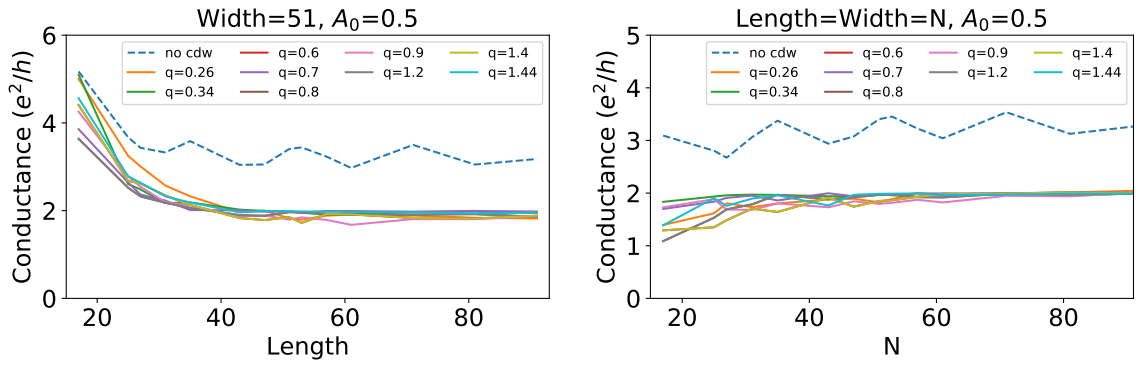


FIGURE 9. Conductance at energy very close to $\omega/2$ as a function of system size for different values of charge-density wave perturbation. This perturbation suppresses the contribution of bulk gapless modes and thus only the quantized contribution from gapless edge modes survive.